Journal of Alloys and Compounds 723 (2017) 820–825

Contents lists available at ScienceDirect

Journal of Alloys and Compounds

journal homepage: http://www.elsevier.com/locate/jalcom

Modification of the optoelectronic properties of Cu_2CdSnS_4 through low-temperature annealing

M. Pilvet [a, *], M. Kauk-Kuusik [a], M. Grossberg [a], T. Raadik [a], V. Mikli [a], R. Traksmaa [b], J. Raudoja [a], K. Timmo [a], J. Krustok [a, c]

[a] Department of Materials and Environmental Technology, Tallinn University of Technology, Ehitajate tee 5, 19086, Tallinn, Estonia
[b] Department of Mechanical and Industrial Engineering, Tallinn University of Technology, Ehitajate tee 5, 19086, Tallinn, Estonia
[c] Division of Physics, Tallinn University of Technology, Ehitajate tee 5, 19086, Tallinn, Estonia

ARTICLE INFO

Article history:
Received 20 March 2017
Received in revised form
26 June 2017
Accepted 27 June 2017
Available online 30 June 2017

Keywords:
Cu_2CdSnS_4
Stannite
Polycrystalline powder
Photoluminescence
Raman scattering
Structural transition

ABSTRACT

In this study the experimental evidence of the existence of Cu-Cd disordering in Cu_2CdSnS_4 is presented. The influence of low-temperature annealing from 100 °C to 400 °C to the optical and structural properties of Cu_2CdSnS_4 polycrystalline powder was studied. Raman scattering and temperature dependent photoluminescence analysis were used to show that the degree of disordering can be reduced with the low-temperature annealing below the critical temperature. According to our study the critical temperature lies in the range from 200 °C to 250 °C. It was found that, the change in the degree of disordering in Cu_2CdSnS_4 is accompanied with the change in the radiative recombination channel related to different type of defect clusters.

1. Introduction

The I_2-II-IV-VI_4 quaternary compounds have attracted considerable interest as potential absorber materials in photovoltaic solar cells due to suitable energy band gaps, high absorption coefficient and earth abundant elements. Solar cells based on Cu_2ZnSnS_4 absorber have achieved the power conversion efficiency as high as 9.2% [1]. Because of the similar properties, Cu_2CdSnS_4 is also considered as possible photovoltaic material. Nitche et al. synthesized single crystal of Cu_2CdSnS_4 by iodine vapor transport and identified the crystal structure as a stannite type $I\bar{4}2m$ [2]. The compound has direct band gap E_g ~1.4 eV and an absorption coefficient larger than 1×10^4 cm^{-1} in the visible range of spectrum [3,4]. According to Shockley–Queisser efficiency limit for solar cells using a single *p-n* junction, the bandgap of Cu_2CdSnS_4 is closer to the ideal bandgap 1.34 eV [5] (using an AM1.5 solar spectrum) than Cu_2ZnSnS_4 (E_g ~ 1.5 eV) to reach higher device efficiency. Cu_2CdSnS_4 is an intrinsic *p*-type semiconductor and the *p*-type conductivity is attributed to Cu vacancies (V_{Cu}) [6] and/or copper in cadmium site (Cu_{Cd}) acceptor defects [7].

Different methods have been studied to prepare Cu_2CdSnS_4 thin films, such as atom beam sputtering [3], solution method [8,9], co-sputtering deposition [10], spin coating [11,12], spray pyrolysis [13], sol-gel method [14], etc. We have used monograin powder technology and reported 2.7% efficiency for pure Cu_2CdSnS_4 solar cells [15]. Recently, we presented improved monograin layer solar cell efficiency of 4.2% at the PVSEC-26 conference. Despite of the suitable material properties the performance of Cu_2CdSnS_4 devices is still low. In Cu_2ZnSnS_4, the main limitation is due to low open circuit voltage (V_{oc}) as compared to the band gap energy value E_g. Recently, it has been shown in several studies [16–18] that the existence of Cu and Zn cation disorder in Cu_2ZnSnS_4 kesterite crystal structure could be one reason for the large open circuit voltage deficit. Main reason for poor performance of Cu_2CdSnS_4 solar cells is not yet clarified and more information about the optoelectronic properties is needed.

Similarly to Cu_2ZnSnS_4, density functional theory calculations in Ref. [7] indicate that the Cu-Cd cation disorder is also possible in Cu_2CdSnS_4. These first principles calculations have shown that the antisite defect Cu_{Cd} and self-compensated defect complex $Cu_{Cd} + Cd_{Cu}$ have very low formation energies, 0.59eV/atom and

* Corresponding author.
E-mail address: Maris.pilvet@ttu.ee (M. Pilvet).

http://dx.doi.org/10.1016/j.jallcom.2017.06.307
0925-8388/

0.21 eV/atom, respectively. It was also shown that the random distribution of different defect pairs induces spatial band gap fluctuations, in the case of $Cu_{Cd} + Cd_{Cu}$ with the depth of about 0.1 eV. Another defect pair $2Cu_{Cd} + Sn_{Cd}$ has also low formation energy and in case of high concentrations it may result in very large band gap fluctuations of about 0.43–0.65 eV [7]. Since these unfavorable defect clusters have very low formation energies throughout all the compositional range of Cu_2CdSnS_4 [7] only thermal treatments could be used to modify the type of prevailing defect clusters. Among single native defects, the calculated acceptor level of Cu_{Cd} is 0.13 eV above the valence band edge. The donor level Cd_{Cu} is shallow (~0.05 eV below the conduction band edge), but Sn_{Cd} is a deep donor (~0.8 eV below the conduction band edge) that may act as electron-hole recombination center [7]. However, there is no experimental evidence of the Cu-Cd cation disorder in Cu_2CdSnS_4 available in literature. Moreover, there is lack of experimental data about the defects and related recombination mechanisms in Cu_2CdSnS_4. This information is of crucial importance for the development of efficient solar cells. In this study we used temperature dependent photoluminescence (PL) spectroscopy and Raman spectroscopy for exploring the optoelectronic properties of Cu_2CdSnS_4 polycrystalline powder that was modified by low-temperature heat-treatments.

2. Experimental

Polycrystalline powder of Cu_2CdSnS_4 was synthesized from elemental Cu (99.9%), Sn (99.9%), S (99.999%) and binary CdS (99.999%) powders by solid-state reaction in sealed evacuated quartz ampoules. For the synthesis, the starting materials were weighted in appropriate metal ratios (Cu: Sn: CdS = 1.85: 1: 1) with addition of sulfur and grounded in an agate mortar. The mixture of precursors was mounted into quartz ampoule, sealed under vacuum and placed in the chamber furnace. The temperature of the furnace was increased from room temperature (RT) to 200 °C with a rate of 10°/min. Sulfurization process of metal components was obtained by keeping the mixture at 200 °C for 24 h. Subsequently, the temperature of the furnace was increased to 900 °C with the rate of 12°/min and powder was homogenized at this temperature for 168 h. A complete homogenization was obtained by decreasing the temperature to 740 °C and keeping the powder at this temperature for 168 h. Finally, the powder was cooled from 740 °C to RT for 19 h.

It has been previously shown that the optoelectronic properties are strongly influenced by the structural disordering in kesterite-type materials [19,20] and the degree of disordering can be reduced by low-temperature annealing treatments below the critical temperature (T_c ~ 260 °C for Cu_2ZnSnS_4 and T_c ~ 200 °C for $Cu_2ZnSnSe_4$) [21,22]. In present study similar low-temperature annealing was applied on Cu_2CdSnS_4 polycrystalline powder to identify the existence of structural disordering and to investigate the corresponding changes in the optical and structural properties of Cu_2CdSnS_4.

For this study, the synthesized polycrystalline powder was ground in an agate mortar and divided to equal amounts to the quartz ampoules, which were subsequently evacuated to 10^{-2} Torr vacuum and sealed with C_3H_8/O_2 flame. All sealed ampoules were heated up to 740 °C, annealed at this temperature for 1 h and then cooled by quenching into cold water. This annealing was done for healing out the mechanical damages on the powder particle surfaces caused by grinding process.

Subsequent low-temperature annealing study was done at following temperatures (T_{ann}): 100 °C, 150 °C, 175 °C, 200 °C, 225 °C, 250 °C, 300 °C, 350 °C and 400 °C for different time periods from 1 h to 2 weeks. After low-temperature annealing, the ampoules were quenched to cold water. Our experiments showed that the stable PL band position was reached by annealing at least 1 week at temperature below 200 °C, annealing at higher temperatures (T_{ann} > 200 °C) needed less time to reach stability. To be sure that the degree of ordering at a given temperature is reached, all powders used for the structural and optical studies were annealed for 1 week.

The structural investigation of the Cu_2CdSnS_4 polycrystalline powders was carried out by X-ray diffraction (XRD) and Raman spectroscopy. XRD patterns of the powders were recorded on a Bruker AXS X-ray diffractometer D5005 using Cu Kα1 radiation (λ = 1.5406 Å) with variable slit V12. Obtained data was analyzed by ICDD PDF 2015 database (International Center for Diffraction Data). Raman spectra were recorded by using the Horiba's LabRam HR800 spectrometer equipped with a multichannel CCD detection system in the backscattering configuration using 532 nm laser line with spot size of 5 μm. The same equipment was used for room temperature photoluminescence (RT-PL) measurements.

The chemical composition of polycrystalline powder was analyzed by energy dispersive X-ray spectroscopy (EDX) using Bruker Esprit 1.8 system. The morphology of crystals was studied with the high-resolution scanning electron microscope (HR-SEM) Zeiss ULTRA 55. EDX mapping was carried out over the polycrystalline surface to investigate the elemental distribution and compositional uniformity over large area and different polycrystals. For low temperature PL measurements, the powder crystals were mounted in the closed–cycle He cryostat and cooled down to 10 K. The 441 nm He-Cd laser line was used for PL excitation and the spectra were detected by using InGaAs detector.

3. Results and discussion

3.1. Results of structural and compositional analysis

The elemental composition of synthesized Cu_2CdSnS_4

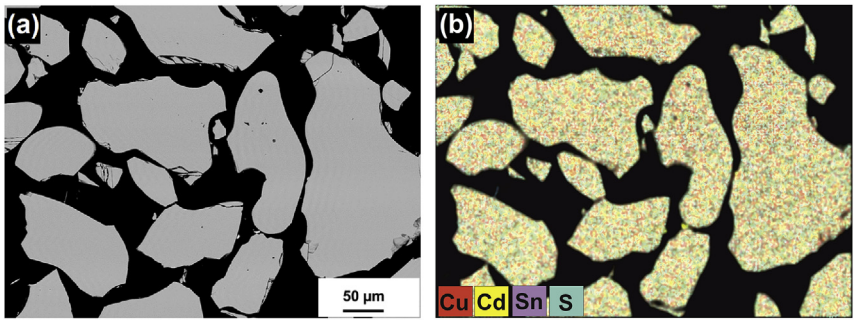

Fig. 1. (a) SEM image of the polished cross-section and (b) elemental mapping by EDX for Cu, Cd, Sn and S of individual Cu_2CdSnS_4 crystals.

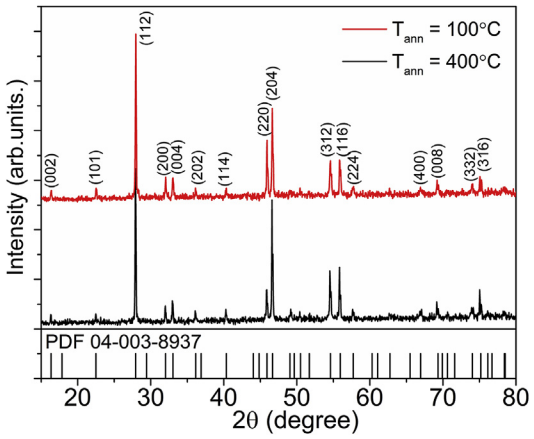

Fig. 2. XRD patterns of the Cu_2CdSnS_4 polycrystals annealed at 100 °C and 400 °C for 1 week.

polycrystalline powder was determined from polished cross-section of individual crystals. Fig. 1 presents SEM micrographs of (a) the polished cross-section and (b) the elemental mapping of Cu, Cd, Sn and S of individual Cu_2CdSnS_4 crystals. Fig. 1b reveals that the elements are homogeneously distributed in the bulk of the powder crystals.

The average bulk composition of synthesized Cu_2CdSnS_4 polycrystalline powder determined by EDX analysis is [Cu] = 24.5 at %, [Cd] = 13.0 at %, [Sn] = 12.5 at % and [S] = 50.0 at %. After different low-temperature annealing experiments, the composition of the powder did not change.

For structural studies, XRD and Raman analysis were performed. The XRD patterns of the Cu_2CdSnS_4 polycrystalline powders annealed at $T_{ann} = 100$ °C and $T_{ann} = 400$ °C, are presented in Fig. 2. The major diffraction peaks can be attributed to (112), (200), (004), (220), (204), (312) and (116) planes of stannite type Cu_2CdSnS_4 with the space group $I\bar{4}2m$ (ICDD PDF 04-003-8937). The *a*- and *c*-lattice constants were calculated from the XRD data and are $a = 5.592$ Å and $c = 10.857$ Å for both samples. All annealed Cu_2CdSnS_4 polycrystalline powders showed similar XRD pattern and no other phases were detected.

Raman spectra of the Cu_2CdSnS_4 polycrystalline powder annealed at $T_{ann} = 100$ °C and $T_{ann} = 400$ °C are presented in Fig. 3. The spectra of Cu_2CdSnS_4 annealed at different temperatures are all similar except for the widths of the peaks and for clearance only the spectra for the material annealed at the lowest ($T_{ann} = 100$ °C) and at the highest temperature ($T_{ann} = 400$ °C) used in this study are presented. The observed Raman spectra are in agreement with previously published data [10,15,23] and the two Raman active A_1 symmetry modes characteristic for the stannite type structured Cu_2CdSnS_4 can be found at 332 cm^{-1} and 283 cm^{-1}. These modes result from the motions of anions only. Other symmetry Raman modes (E and B_2 modes) were detected at 89 cm^{-1}, 138 cm^{-1}, 237 cm^{-1}, 268 cm^{-1}, 343 cm^{-1}, 352 cm^{-1} and 364 cm^{-1}.

No significant difference in the Raman peak positions of Cu_2CdSnS_4 polycrystalline powder annealed at different temperatures could be detected. From the inset graph in Fig. 3 a clear tendency towards increasing full width at the half maximum (FWHM) of the dominating A_1 mode with increasing annealing temperature can be seen. It has been shown that in kesterite Cu_2ZnSnS_4 and $Cu_2ZnSnSe_4$ the low-temperature annealing at different temperatures below and above the critical temperature leads to the changes in the degree of Cu-Zn ordering and in the width and symmetry of the A_1 Raman peak [21,22,24,25]. Broadening of the A_1 Raman peak with increasing annealing temperature was observed and attributed to the higher degree of disordering. It was found that the asymmetry of the A_1 peak is caused by a shoulder peak at low wavenumber side that was attributed to the A_1 mode of the disordered Cu_2ZnSnS_4. The same trend as was seen in Cu_2ZnSnS_4 is observed in present study for Cu_2CdSnS_4 indicating higher level of disordering with increasing annealing temperature. An example of the fitting of the A_1 Raman peak of Cu_2CdSnS_4 annealed at $T_{ann} = 100$ °C and $T_{ann} = 400$ °C with two Lorentzian peaks is shown in Fig. 4. The shoulder peak at the low wavenumber side at 331 cm^{-1} can be attributed to the disordered Cu_2CdSnS_4 and its relative intensity decreases with decreasing annealing temperature.

3.2. Photoluminescence analysis results

To determine the influence of low-temperature annealing to the defect structure of Cu_2CdSnS_4 temperature dependent photoluminescence (PL) measurements were performed. PL spectroscopy is non-contact and one of the most sensitive tools for studying the defects in semiconductors. Low temperature ($T = 10$ K) PL spectra of all studied Cu_2CdSnS_4 polycrystalline powders annealed at different temperatures consist of one broad asymmetric PL band, see Fig. 5. We observe a shift in the PL band position towards lower energies with increasing annealing temperature. The highest energy PL band is situated at 1.215 eV corresponding to the Cu_2CdSnS_4

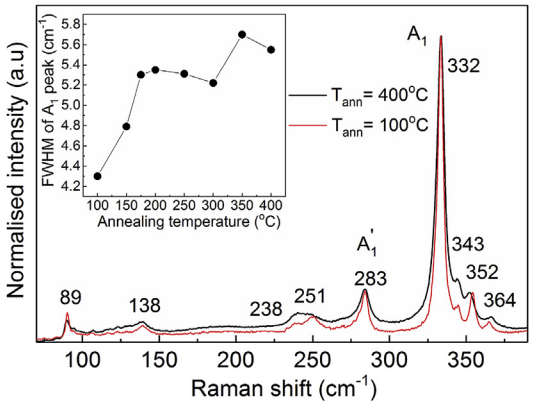

Fig. 3. Raman spectra of Cu_2CdSnS_4 annealed at temperatures 100 °C and 400 °C for 1 week. The inset graph shows the dependence of the FWHM of the A_1 Raman mode at 332 cm^{-1} on the annealing temperature.

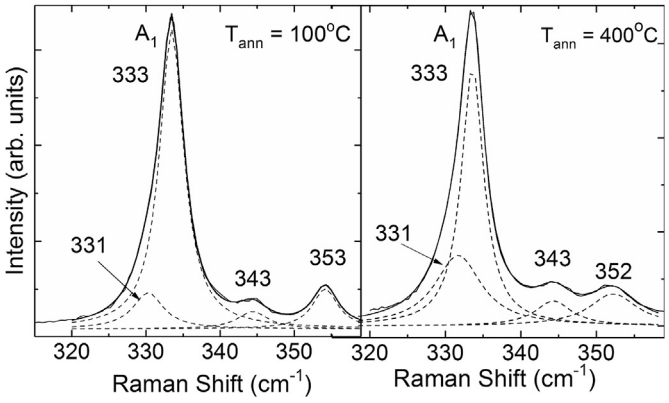

Fig. 4. Fitting of the A_1 Raman peak of Cu_2CdSnS_4 annealed at 100 °C and 400 °C for 1 week, with two Lorentzian peaks. The shoulder peak at the low wavenumber side at 331 cm^{-1} can be attributed to the disordered Cu_2CdSnS_4.

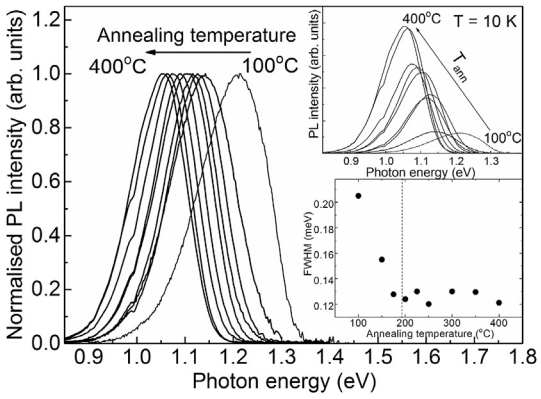

Fig. 5. The normalized low-temperature (T = 10 K) PL spectra of Cu_2CdSnS_4 polycrystalline powders annealed at different temperatures in the range from 100 °C to 400 °C for 1 week. A shift of the PL band towards lower energies with increasing annealing temperature can be seen. The upper inset graph presents the original PL spectra showing the decrease in the PL intensity with decreasing annealing temperature. In the lower inset graph, the dependence of the FWHM of the PL band on the annealing temperature is shown.

polycrystalline powder annealed at 100 °C for 1 week (sample will be named as "ordered" based on the Raman results). The lowest energy PL band is detected at 1.064 eV corresponding to the Cu_2CdSnS_4 polycrystalline powder annealed at 400 °C for 1 week (sample will be named as "disordered").

The overall difference in the PL band positions of the ordered and disordered Cu_2CdSnS_4 is about 150 meV. As can be seen from the upper inset graph in Fig. 5, the intensity of the PL signal decreases with decrease in the annealing temperature. In addition, narrowing of the PL band is observed for higher annealing temperatures, the full width at the half maximum (FWHM) being largest for the lowest annealing temperature (T_{ann} = 100 °C), see lower inset graph in Fig. 5. Two regions were observed in the dependence of the FWHM on the annealing temperature: above T_{ann} = 200 °C, the FWHM is almost constant ranging from 0.12 to 0.13 meV, and below T_{ann} = 200 °C the FWHM increases up to 0.16 eV with decreasing annealing temperature. It is also important to notice that the PL bands are located more than 0.2 eV below the bandgap energy of Cu_2CdSnS_4 that is reported to be 1.4 eV at room temperature [15] and is even higher at low temperature (T = 10 K).

In order to determine the recombination mechanisms behind the PL bands temperature dependent PL measurements were performed. Due to the asymmetric shape of the PL bands, all the spectra were fitted with empirical asymmetric double sigmoid function [26] that describes well such broad and asymmetric PL bands with exponential tail in the low-energy side that are very common in multinary compound semiconductors with spatial potential fluctuations. The spatial potential fluctuations result from high concentration of randomly distributed charged native defects [25–27]. The asymmetric shape results from the band tails of the density of states function extending into the band gap. The average depth of the fluctuations γ can be determined from the slope of the low energy side of the PL band [26–28]. The corresponding γ values of the PL bands of the Cu_2CdSnS_4 polycrystalline powders annealed at different temperatures can be found in Table 1 and it was found that the average depth of the fluctuations is very similar in all samples indicating to similar large defect concentrations.

From the temperature dependencies of the PL spectra the temperature dependence of the PL band maxima and integrated intensity were analyzed. It was found that the PL bands measured from the Cu_2CdSnS_4 polycrystalline powders annealed at temperatures below T_{ann} = 200 °C are composed of two PL bands that are labeled #1 and #2 (an example of the fitting of the spectra is presented in Fig. 6). The presence of two PL bands also explains the widening of the PL spectrum with decreasing annealing temperature. From the Arrhenius plots the thermal activation energies of the quenching of the PL bands were determined by using the theoretical expression for discrete energy levels for fitting [29]:

$$\phi(T) = \frac{\phi_0}{1 + \alpha_1 T^{3/2} + \alpha_2 T^{3/2} \exp(-E_r/kT)}, \quad (1)$$

where Φ is integrated intensity, α_1 and α_2 are the process rate parameters and E_T is the thermal activation energy. The obtained values of the thermal activation energies E_T in dependence of the annealing temperature are listed in Table 1 together with the positions of the PL band maxima and FWHM. Two annealing temperature regions can be observed: two PL bands were detected in Cu_2CdSnS_4 annealed at temperatures below T_{ann} = 200 °C showing thermal activation energies of around 60 meV and 110 meV, and one PL band was observed in Cu_2CdSnS_4 annealed at temperatures above T_{ann} = 200 °C having high thermal activation energy above 130 meV.

It has been shown that in disordered Cu_2ZnSnS_4 recombination mechanism involving defect clusters inducing local bandgap energy shrinkage is dominating [24]. The latter results in large band gap fluctuations that create efficient recombination paths for photogenerated carriers in the material. In ordered Cu_2ZnSnS_4 recombination involving deep acceptor defects (>200 meV) is prevailing at low temperatures [24]. Similarly, high concentration of $Cu_{Cd} + Cd_{Cu}$ and $2Cu_{Cd} + Sn_{Cd}$ defect complexes is predicted in Cu_2CdSnS_4 [7], being responsible for the Cu-Cd disordering. According to the theoretical calculations, the difference in the bandgap energies of disordered and ordered Cu_2CdSnS_4 is about 100 meV [7]. Therefore, recombination mechanism involving defect clusters is also expected in this material.

Considering that the bandgap energy of Cu_2CdSnS_4 at low

Table 1
Parameters describing the low temperature PL bands of the Cu_2CdSnS_4 polycrystalline powders annealed at different temperatures: γ – average depth of the spatial potential fluctuations, $h\nu_{max}$ – PL band peak position, E_T - thermal activation energy and FWHM – full width at the half maximum of the PL band. For two samples (175 °C and 300 °C, temperature dependencies were not measured).

Annealing temperature (°C)	γ (meV)	$h\nu_{max\#1}$ (eV)	$E_{T\#1}$ (meV)	FWHM(#1) (eV)	$h\nu_{max\#2}$ (eV)	$E_{T\#2}$ (meV)	FWHM(#2) (eV)
100	23	1.165	110 ± 4	0.13	1.245	60 ± 5	0.10
150	22	1.123	105 ± 6	0.13	1.189	62 ± 7	0.11
175	24	1.112	–	0.12	1.161	–	0.11
200	25	1.116	86 ± 8	0.12			
225	24	1.106	146 ± 7	0.13			
250	25	1.093	135 ± 7	0.12			
300	26	1.079	–	0.13			
350	27	1.065	151 ± 7	0.13			
400	27	1.064	133 ± 5	0.12			

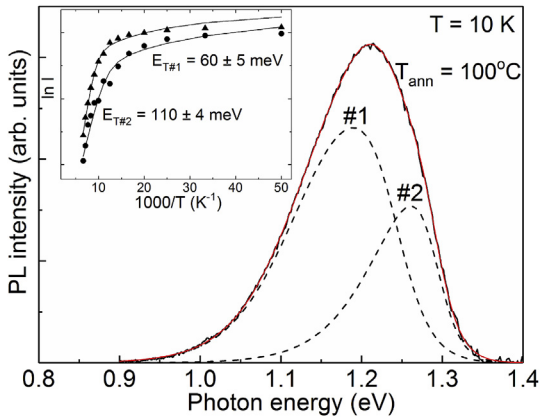

Fig. 6. The low-temperature (T = 10 K) PL spectrum of Cu_2CdSnS_4 polycrystalline powder annealed at 100 °C for 1 week together with the fitting result. The inset graph presents the Arrhenius plots for the two PL bands used for determining the thermal quenching activation energies for #1 and #2.

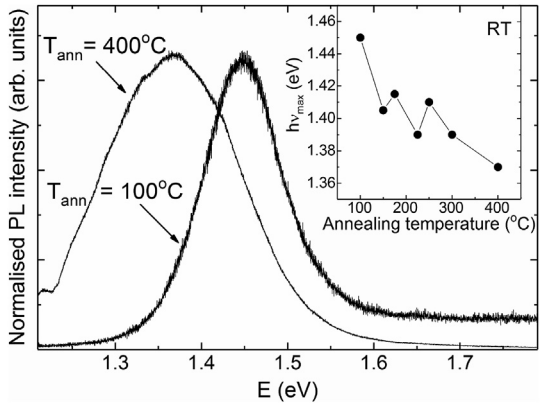

Fig. 7. RT- PL spectra of Cu_2CdSnS_4 annealed at temperatures 100 °C and 400 °C for 1 week. The shift of the position of the PL band maximum towards lower energies with increasing annealing temperature is detected.

temperatures is close to 1.5 eV, the PL bands are very far from the band edge, separation of the PL band from the band gap is over 300 meV and over 200 meV for #1 and #2, respectively. Different thermal activation energies of the PL band quenching were found for #1 (above 100 meV) and #2 (below 100 meV), indicating to a different recombination channel. Considering the thermal activation energies and the PL band positions with respect to the low temperature bandgap energy of Cu_2CdSnS_4, one can see that in both ordered and disordered Cu_2CdSnS_4 the dominating radiative recombination is related to the defect clusters inducing bandgap energy shrinkage that was also seen in disordered Cu_2ZnSnS_4 [30]. However, the dominating defect clusters are different in ordered and disordered Cu_2CdSnS_4. We propose that in disordered Cu_2CdSnS_4 the $2Cu_{Cd} + Sn_{Cd}$ defect complexes inducing large bandgap energy fluctuations (with depth > 0.4 eV [7]) dominate. In ordered material the coexistence of $2Cu_{Cd} + Sn_{Cd}$ and $Cu_{Cd} + Cd_{Cu}$ defect complexes is present resulting in the two observed PL bands #1 and #2. However, based on the PL intensity analysis (see upper inset graph in Fig. 5) the overall concentration of the mentioned defect complexes is reduced in ordered material.

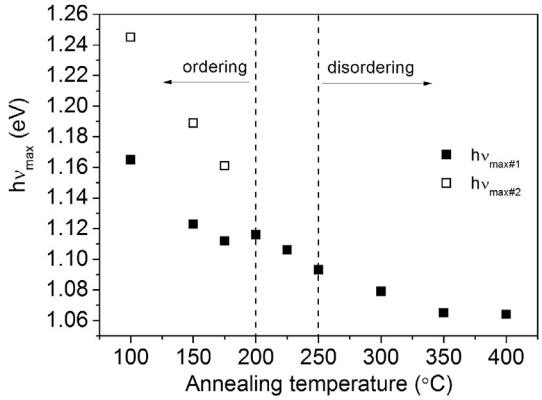

Fig. 8. PL band positions of Cu_2CdSnS_4 polycrystalline powders depending on the low-temperature annealing in the range from 100 °C to 400 °C for 1 week.

RT-PL measurements were also performed to the Cu_2CdSnS_4 polycrystalline powders annealed at different temperatures. Similarly to low-temperature PL (10 K) results a shift of the PL band towards lower energies with increasing annealing temperature was observed, the positions of the PL bands being 1.45 eV and 1.37 eV for samples annealed at 100 °C and 400 °C, respectively. For clearance, only the spectra of ordered and disordered Cu_2CdSnS_4 (e.g. annealing temperatures 100 °C and 400 °C) is presented in Fig. 7. Much broader PL band is observed for the disordered material, most probably caused by larger band gap fluctuations. Considering the room temperature bandgap energy of Cu_2CdSnS_4 around 1.4 eV [3,4], the observed PL bands result from the band-to-band recombination. Notice, that it is not the same PL band that was observed at low temperature (10 K).

Finally, Fig. 8 shows low-temperature PL band position of Cu_2CdSnS_4 depending on the annealing temperature in the range from 100 °C to 400 °C for 1 week. The vertical dashed lines in Fig. 8 indicate to the annealing temperature region where the PL band position is almost constant and change in the recombination mechanism has not yet taken place. Almost constant FWHM of the A_1 Raman mode was observed in the same annealing temperature region from 200 °C to 250 °C. We can conclude that it is possible to modify the degree of disordering with the low-temperature annealing treatments below the critical temperature that according to our study lies in the temperature range from 200 °C to 250 °C.

4. Conclusions

From the Raman scattering and temperature dependent PL analysis of the Cu_2CdSnS_4 polycrystalline powder we can conclude that the Cu-Cd disordering predicted by the theoretical first principles calculations [7] is present in this material. We have shown in this study that the degree of disordering can be reduced with the low-temperature annealing treatments below the critical temperature that according to our study lies in the temperature range from 200 °C to 250 °C. It was found the change in the degree of disordering in Cu_2CdSnS_4 is accompanied with the change in the radiative recombination channel related to different type of defect clusters.

Acknowledgements

This work was supported by institutional research funding IUT (IUT19-28) of the Estonian Ministry of Education and Research, by the European Union through the European Regional Development Fund, Project TK141, and by FP7 Project CHEETAH Grant Agreement No. 609788.

References

[1] T. Kato, H. Hiroi, N. Sakai, S. Muraoka, H. Sugimoto, Characterization of front

and back interface on Cu_2ZnSnS_4 thin-film solar cells, in: Proc. of 27th EU-PVSEC, 2012, pp. 2236–2239. http://dx.doi.org/10.4229/27thEUPVSEC2012-3CO.4.2.
[2] W. Schäfer, R. Nitsche, Tetrahedral quaternary chalcogenides of the type Cu_2–II–IV–$S_4(Se_4)$, Mater. Res. Bull. 9 (1974) 645–654. http://dx.doi.org/10.1016/0025-5408(74)90135-4.
[3] K. Ito, T. Nakazawa, Electrical and optical properties of stannite-type quaternary semiconductor thin films, Jpn. J. Appl. Phys. 27 (1988) 2094–2097. http://iopscience.iop.org/article/10.1143/JJAP.27.2094/pdf.
[4] H. Matsushita, T. Ichikawa, A. Katsui, Structural, thermodynamical and optical properties of Cu_2-II-IV-VI_4 quaternary compounds, J. Mater. Sci. 40 (2005) 2003–2005. http://doi.org/10.1007/s10853-005-1223-5.
[5] S. Rühle, Tabulated values of the Shockley-Queisser limit for single junction solar cells, Sol. Energy 130 (2016) 139–147. http://dx.doi.org/10.1016/j.solener.2016.02.015.
[6] L. Meng, Y. Li, B. Yao, Z.-H. Ding, G. Yang, R.-J. Liu, R. Deng, L. Liu, Mechanism of effect of intrinsic defects on electrical and optical properties of Cu_2CdSnS_4: an experimental and first-principles study, J. Phys. D. Appl. Phys. 48 (2015), 445005 (7pp), https://doi.org/10.1088/0022-3727/48/44/445105.
[7] Z.-K. Yuan, S. Chen, H. Xiang, X.-G. Gong, A. Walsh, J.-S. Park, I. Repins, S.-H. Wei, Engineering solar cell absorbers by exploring the band alignment and defect disparity: the case of Cu- and Ag-based kesterite compounds, Adv. Funct. Mater. 25 (2015), 6766–6743, http://dx.doi.org/10.1002/adfm.20152272.
[8] H. Guan, J. Zhao, X. Wang, F. Yu, Cu_2CdSnS_4 thin film prepared by a simple solution method, Chalcogenide Lett. 10 (10, October) (2013) 367–372.
[9] W. Zhao, G. Wang, Q. Tian, L. Huang, S. Gao, D. Pan, Solution-processed $Cu_2CdSn(S,Se)_4$ thin film solar cells, Sol. Energy Mater. Sol. Cells 133 (February) (2015) 15–20. http://dx.doi.org/10.1016/j.solmat.2014.10.040.
[10] H. Guo, Y. Li, X. Fang, K. Zhang, J. Ding, Co-sputtering deposition and optical-electrical characteristic of Cu_2CdSnS_4 thin films for use in solar cells, Mater. Lett. 162 (1) (2016) 97–100. http://dx.doi.org/10.1016/j.matlet.2015.09.112.
[11] A.S. Ibraheam, Y. Al-Douri, U. Hashim, D. Prakash, K.D. Verma, M. Ameri, Fabrication, analysis and characterization of $Cu_2Zn_{1-x}Cd_xSnS_4$ quinternary alloy nanostructures deposited on GaN, J. Mater. Sci. 51 (14) (2016) 6876–6885, http://dx.doi.org/10.1007/s10853-016-9975-7.
[12] A.A. Odeh, Y. Al-Douri, R.M. Ayub, A.S. Ibraheam, Ultrasonic effect on optical, topographical and morphological studies of Cu_2CdSnS_4 quaternary alloy nanostructures, J. Alloys Compd. 686 (2016) 883–895. http://dx.doi.org/10.1016/j.jallcom.2016.06.235.
[13] L. Nie, S. Liu, Y. Chai, R. Yuan, Spray pyrolysis deposition and photoresponse of Cu_2CdSnS_4 thin films, J. Anal. Appl. Pyrolysis 112 (2015) 363–368. http://dx.doi.org/10.1016/j.jaap.2014.12.020.
[14] A.S. Ibraheam, Y. Al-Douri, U. Hashim, M.R. Ghezzar, A. Addou, W.K. Ahmed, Cadmium effect on optical properties of $Cu_2Zn_{1-x}Cd_xSnS_4$ quinternary alloys nanostructures, Sol. Energy 114 (2015) 39–50. http://dx.doi.org/10.1016/j.solener.2015.01.018.
[15] K. Timmo, M. Kauk-Kuusik, M. Altosaar, J. Raudoja, T. Raadik, M. Grossberg, T. Varema, M. Pilvet, I. Leinemann, O. Volobujeva, E. Mellikov, Novel Cu_2CdSnS_4 and $Cu_2ZnGeSe_4$ absorber materials for monograin layer solar cell applications, Proceedings of the 28th European Photovoltaic Solar Energy Conference and Exhibition, Paris, France (September 30–October 04 2013), p. 2385, DOI: 10.4229/28thEUPVSEC2013-3BV.6.14.
[16] S. Bourdais, C. Choné, B. Delatouche, A. Jacob, G. Larramona, C. Moisan, A. Lafond, F. Donatini, G. Rey, S. Siebentritt, A. Walsh, G. Dennler, Is the Cu/Zn disorder the main culprit for the voltage deficit in kesterite solar cells? Adv. Energy Mater. (2016) 1502276. http://dx.doi.org/10.1002/aenm.201502276.
[17] G. Krämmer, C. Huber, T. Schnabel, C. Zimmermann, M. Lang, E. Ahlswede, H. Kalt, M. Hetterich, Order-disorder related band gap changes in $Cu_2ZnSn(S,Se)_4$: impact on solar cell performance, in: Proc. 42nd IEEE Photovoltaic Specialist Conference (PVSC), 2015. http://dx.doi.org/10.1109/PVSC.2015.7356096.
[18] K. Timmo, M. Kauk-Kuusik, M. Pilvet, T. Raadik, M. Altosaar, M. Danilson, M. Grossberg, J. Raudoja, K. Ernits, Influence of order-disorder in Cu_2ZnSnS_4 powders of monograin layer solar cells, Thin Solid Films (2016). http://dx.doi.org/10.1016/j.tsf.2016.10.017.
[19] M. Grossberg, J. Krustok, J. Raudoja, T. Raadik, The role of structural properties on deep defect states in Cu_2ZnSnS_4 studied by photoluminescence spectroscopy, Appl. Phys. Lett. 101 (2012) 102102. http://dx.doi.org/10.1063/1.4750249.
[20] T. Raadik, J. Krustok, M. Kauk-Kuusik, k. Timmo, M. Grossberg, K. Ernits, J. Bleuse, Low temperature time resolved photoluminescence in ordered and disordered Cu_2ZnSnS_4 single crystals, Phys. B 508 (2017) 47–50. http://dx.doi.org/10.1016/j.physb.2016.12.011.
[21] G. Rey, A. Redinger, J. Sendler, T.P. Weiss, M. Thevenin, M. Guennou, B. El Adiband, S. Siebentritt, The band gap of $Cu_2ZnSnSe_4$: effect of order-disorder, Appl. Phys. Lett. 105 (2014) 112106. http://dx.doi.org/10.1063/1.4896315.
[22] J.J.S. Scragg, L. Choubrac, A. Lafond, T. Ericson, C. Platzer-Björkman, A low-temperature order-disorder transition in Cu_2ZnSnS_4 thin films, Appl. Phys. Lett. 104 (2014) 041911. http://dx.doi.org/10.1063/1.4863685.
[23] M. Pilvet, M. Kauk-Kuusik, M. Altosaar, M. Grossberg, M. Danilson, K. Timmo, A. Mere, V. Mikli, Compositionally tunable structure and optical properties of $Cu_{1.85}(Cd_xZn_{1-x})_{1.1}SnS_{4.1}$ ($0 \leq x \leq 1$) monograin powders, Thin Solid Films 582 (2015) 180. http://dx.doi.org/10.1016/j.tsf.2014.10.091.
[24] T. Gürel, C. Sevik, T. Cagin, Characterization of vibrational and mechanical properties of quaternary compounds Cu_2ZnSnS_4 and $Cu_2ZnSnSe_4$ in kesterite and stannite structures, Phys. Rev. B 84 (2011) 205201. https://doi.org/10.1103/PhysRevB.84.205201.
[25] M. Grossberg, J. Krustok, T. Raadik, M. Kauk-Kuusik, J. Raudoja, Photoluminescence study of disordering in the cation sublattice of Cu2ZnSnS4, Curr. Appl. Phys. 14 (2014) 1424–1427. http://dx.doi.org/10.1016/j.cap.2014.08.013.
[26] J. Krustok, H. Collan, M. Yakushev, K. Hjelt, The role of spatial potential fluctuations in the shape of the PL bands of multinary semiconductor compounds, Phys. Scr. T79 (1999) 179–182. http://iopscience.iop.org/1402-4896/1999/T79/041.
[27] M. Grossberg, J. Krustok, K. Timmo, M. Altosaar, Radiative recombination in $Cu_2ZnSnSe_4$ monograins studied by photoluminescence spectroscopy, Thin Solid Films 517 (2009) 2489–2492. http://dx.doi.org/10.1016/j.tsf.2008.11.024//.
[28] A.P. Levanyuk, V.V. Osipov, Edge luminescence of direct-gap semiconductors, Sov. Phys. Usp. 24 (1981) 187–215. https://doi.org/10.1070/PU1981v024n03ABEH004770.
[29] J. Krustok, H. Collan, K. Hjelt, Does the low temperature Arrhenius plot of the photoluminescence intensity in CdTe point towards an erroneous activation energy? J. Appl. Phys. 81 (1997) 1442–1445. http://dx.doi.org/10.1063/1.363903.
[30] S. Chen, X.G. Gong, A. Walsh, S.-H. Wei, Crystal and electronic band structure of Cu_2ZnSnX_4 (X=S and Se) photovoltaic absorbers: first-principles insights, Appl. Phys. Lett. 94 (2009) 041903. http://dx.doi.org/10.1063/1.3074499.